PAPER • OPEN ACCESS

Waveform retracking of satellite radar altimeter based on singular spectrum analysis

To cite this article: Jinyun Guo *et al* 2019 *IOP Conf. Ser.: Earth Environ. Sci.* **237** 032024

IOP Conf. Series: Earth and Environmental Science **237** (2019) 032024 doi:10.1088/1755-1315/237/3/032024

Waveform retracking of satellite radar altimeter based on singular spectrum analysis

Jinyun Guo[1*], Wenqiang Di[1], Jiajia Yuan[1], Yupeng Niu[1] and Zhen Li[1]

[1] College of Geodesy and Geomatics, Shandong University of Science and Technology, Qingdao, Shandong Province, 266590, China

[*]Corresponding author's e-mail: jinyunguo1@126.com

Abstract. Satellite altimetric waveform retracking plays an important role in improving the accuracy of altimetry data, and three retracking methods had been analyzed. A waveform series was constructed, and the SSA (singular spectrum analysis) was introduced to process waveform series to denoise and reconstruct waveform series. Three retracking methods, which were OCOG, threshold and function fitting method, were used to retrack reconstructed waveforms to correct GDR data. The waveform data of Jason-1 satellite in South China sea were selected to constructe waveform series to denoise and reconstruct by SSA. The reconstructed waveforms became more regular, and the leading edge of single waveform was more easily recognized. The result showed that combining SSA and retracking methods to process waveform data could improve the value of IMP(improvement percentage) compared to using retracking methods merely, which proved that this new method could improve the altimetric accuracy and could be further studied and applied.

1. Introduction

Satellite altimetry is widely used in many subjects with its all-weather, periodic and real-time synchronization advantages[1-2]. It uses the altimeter carried on the satellite to measure the distance from the satellite to the subpoint to determine the SSH (sea surface height). Due to the improvement of the accuracy of instrument correction, atmospheric refraction correction, geophysical environment correction and other error corrections, waveform retracking correction became the key to improve the measurement accuracy of satellite altimetry.

Domestic and foreign scholars had proposed a variety of waveform retracking methods, which were mainly divided into statistical methods[3-6], function fitting methods[7-8] and algorithms based on sub-waveform analysis[9-10]. These methods had achieved good results in certain sea areas, but they had not processed the noise contained in the waveforms, nor had they studied the entire waveform series. SSA is a mathematical statistical analysis method, which is suitable for single time series analysis. For the data which physical essence is unknown, SSA can extract as much reliable information as possible from its finite-length observation series, and it can be used to trend identification, cycle judgment, denoise processing and data reconstruction[11]. This method had been widely used in oceanography, meteorology and surveying and many other fields[12-15]. The waveform data on one track are suitable for constructing a time series, and this waveform series is characterized by periodic oscillation, which is suitable for analysis with SSA.

In order to improve the quality of satellite altimetry data, this paper proposed a new method that combined SSA and waveform retracking algorithm to process waveform data. The Jason-1 20hz waveform data in the southwestern area of Taiwan were selected to construct waveform series, and

SSA was used to process waveform series and obtained reconstruction series. Retracked original waveform and reconstructed waveform and calculated the SSH respectively, and then calculated the IMP value and compared the size[16].

2. SSA and retracking methods of waveforms

2.1SSA

This paper first constructed waveform series from waveform data, and performed SSA on the series. The following describes the specific process[11].

(1) Construct time-delay matrix. For a well-constructed one-dimensional waveform series with the length of N, $x_1, x_2, \cdots, x_N$, select the appropriate window length L ($1 < L < \frac{N}{2}$), and construct the time-delay matrix X

$$X = \begin{bmatrix} x_1 & x_2 & \cdots & x_{N-L+1} \\ x_2 & x_3 & \cdots & x_{N-L+2} \\ \vdots & \vdots & \ddots & \vdots \\ x_L & x_{L+1} & \cdots & x_N \end{bmatrix} \tag{1}$$

(2) Singular value decomposition. The self-covariance matrix of matrix X is $T_X = X \bullet X^T$, and the every element of T_X is $T_{ij} = \frac{1}{N-k}\sum_{t=1}^{N-K} x_t x_{t+k}$, where $i, j = 1, 2, \cdots, L$, and $k = |i - j|$. The eigenvalues of T_X is λ_i, where $i = 1, 2, \cdots, L$. Sort the eigenvalues by size is $\lambda_1 \ge \lambda_2 \ge \cdots \ge \lambda_L$, and the corresponding eigenvector is $u_1, u_2, \cdots, u_L$. The singular value decomposition of matrix X can be expressed as

$$x(i, j) = \sum_{K=1}^{L} v(i, k) u(k, j) \tag{2}$$

In the formula, $i = 1, 2, \cdots, N - L + 1; j = 1, 2, \cdots, L$; The eigenvector $u(k, j)$ is called the T-EOF (time empirical orthogonal function) of X, and the projection $v(i, k)$ of the waveform series on $u(k, j)$ is called T-PC (time principal component).

(3) Reconstruction. The *i*th RC (reconstruction component) obtained by SSA is

$$x_i^k = \begin{cases} \frac{1}{i}\sum_{j=1}^{i} v(i-j, k) u(k, j), & 1 \le i \le L-1 \\ \frac{1}{L}\sum_{j=1}^{L} v(i-j, k) u(k, j), & L \le i \le N-L+1 \\ \frac{1}{N-i+1}\sum_{j=i-N+L}^{L} v(i-j, k) u(k, j), & N-L+2 \le i \le N \end{cases} \tag{3}$$

The proportion of each RC in original waveform series can be expressed by the variance contribution rate $\lambda_i / \sum_{i=1}^{L} \lambda_i$, the variance contribution rate of the first r RCs can be expressed as $\sum_{i=1}^{r} \lambda_i / \sum_{i=1}^{L} \lambda_i$.

2.2OCOG algorithm

OCOG calculates the statistic of a single waveform, including amplitude, width, and the center of gravity, and then obtains the midpoint of the leading edge[3]. The specific calculation formula is

$$A=\left(\sum_{i=1+n}^{N-n}P_i^4(t)\,/\sum_{i=1+n}^{N-n}P_i^2(t)\right)^{1/2} \tag{4}$$

$$W=\left(\sum_{i=1+n}^{N-n}P_i^2(t)\right)/\sum_{i=1+n}^{N-n}P_i^4(t) \tag{5}$$

$$G_{COG}=\sum_{i=1+n}^{N-n}iP_i^2(t)\,/\sum_{i=1+n}^{N-n}P_i^2(t) \tag{6}$$

$$LEP=G_{COG}-{W}/{2} \tag{7}$$

Where N is the total number of gates, n is the number of deviation gates that need to be deleted, $P_i(t)$ is the i-th gate power value, A is amplitude, W is width, G is the center of gravity, and LEP is the midpoint of the leading edge.

2.3 5-β parameter algorithm

The 5-β parameter algorithm selects an appropriate parameter function to fit the altimeter waveform, and obtains the midpoint of leading edge by solving the corresponding parameter[8]. The selected function is

$$y(t)=\beta_1+\beta_2\left(1+\beta_5 Q\right)P\left(\frac{t-\beta_3}{\beta_4}\right) \tag{8}$$

$$Q=\begin{cases}0 & t<\beta_3+0.5\beta_4\\ t-\left(\beta_3+0.5\beta_4\right) & t\geq\beta_3+0.5\beta_4\end{cases} \tag{9}$$

$$P(x)=\int_{-\infty}^{x}\frac{1}{\sqrt{2\pi}}\exp\left(\frac{-q^2}{2}\right)dq \tag{10}$$

Where β_1 is the thermal noise, β_2 is the waveform amplitude, β_3 is the midpoint of leading edge, β_4 is the width of leading edge, β_5 is the slope of trailing edge. Their initial values are given by OCOG.

2.4Threshold algorithm

This method first obtains the waveform amplitude from OCOG and then estimates the thermal noise level at the leading edge of the waveform

$$P_n=\frac{1}{5}\sum_{i}^{i+4}P_i \tag{11}$$

Where i is the first waveform sample gate number. The threshold level is

$$TL=\left(A-P_N\right)\times Th+P_N \tag{12}$$

In the formula, Th is threshold factor, which is a percentage coefficient of the waveform amplitude. According to the two waveform sampling amplitudes before and after TL, the midpoint of the leading edge can be obtained by linear interpolation method.

$$n_{ret}=(\hat{n}-1)+\frac{TL-WD_{\hat{n}-1}}{WD_{\hat{n}}-WD_{\hat{n}-1}} \tag{13}$$

Where n_{ret} represents the midpoint of leading edge after waveform retracking, $WD_{\hat{n}}$ is the waveform sampling power just above the TL, and $\hat{n}$ is the gate corresponding to $WD_{\hat{n}}$. When the altimeter echo is dominated by ocean waveforms, Th takes 50%, and When non-marine waveforms are more, Th takes 30%[17].

3. Experimental results and analysis

3.1Research data selection

The Jason-1 satellite was a marine altimeter satellite, which had the same ground tracks with the T/P satellite. It carried on Poseidon-2 altimeter, and its measurement accuracy reached centimetre level in the deep sea area. This paper selected the sea area in the southwestern part of Taiwan island as the experimental area, and the area was shown in Figure 1. Jason-1 had many passes passing through this area, and the Pass051 of Cycle060 was selected as the research object. The latitude span was 19.5~22.5 degree. The average depth of this sea area was more than 2000m, and the deepest point was 3400m. Jason-1 satellite had multiple versions of data, and this paper selected its SGDR-E version Ku band 20hz waveform data, which could be downloaded from AVISO official website (http://www.aviso.altimetry.fr/en/data.html).

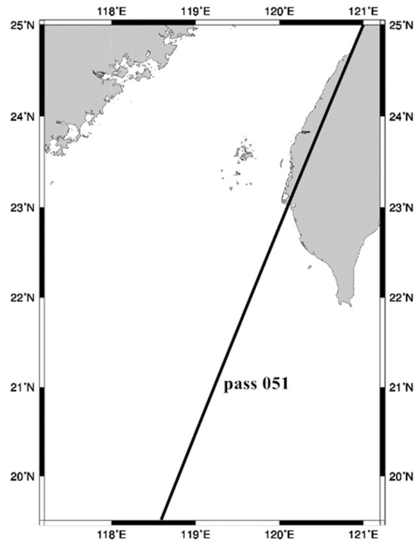

Figure 1. Cycle60 pass051 ground track in South China sea.

3.2SSA

Pass051 was an ascending pass, and the waveforms data of Pass051 were arranged in ascending order to construct a waveform series. Used SSA to process the constructed waveform series. The selection of the length of the window was important, generally taking an integer multiple of the period[18]. Since Jason-1 satellite had 104 gates in one waveform, the window length L was 1040 in this study. For the separated subsequence RCs, the reconstruction order was selected according to the w-correlation method and the variance contribution rate[18]. The result was shown in Figure 2.

As shown in Figure 2, there were greater correlation from the eleventh RCs, indicating these RCs from the eleventh items contained large noise and the variance contribution rate of the first eleventh RCs was 97.32%. Selected the first eleventh RCs to reconstruct waveform series, and the comparison between original waveform and reconstructed waveform was shown in Figure 3.

It could be seen from Figure 3 that the reconstructed waveform conformed to the characteristics of the ocean waveform, and its leading edge portion was more obvious, and the slope was changed. The trailing edge oscillation became smaller, and the front and rear ends of the waveform appeared similar enveloping phenomenon due to SSA. The single waveform's front and rear end gates needed to be deleted when retracked it. In this paper, ten gates were deleted at the front and rear end respectively. The corresponding original waveform series and reconstructed waveform series were shown in Figure 4 and Figure 5.

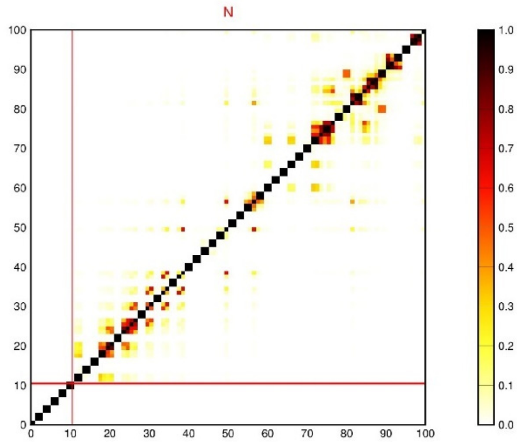

Figure 2. W-correlation of the first 100 RCs.

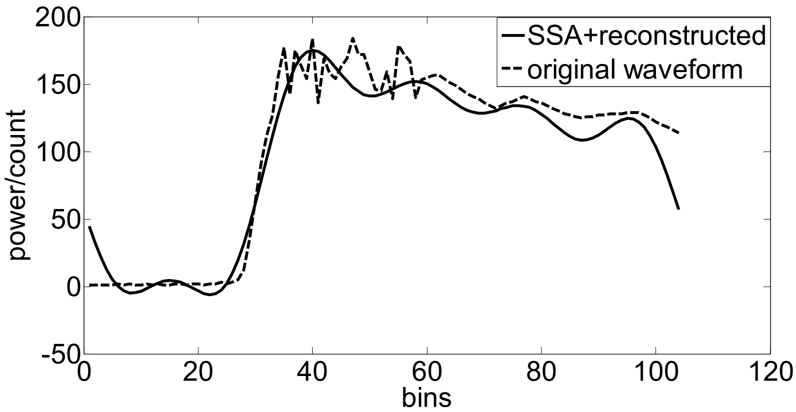

Figure 3. Comparison between original waveform and reconstructed waveform.

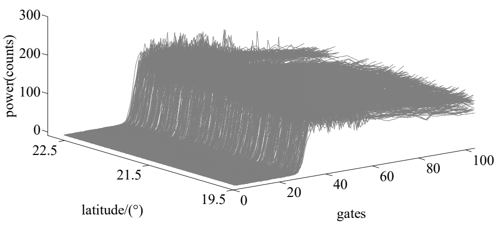

Figure 4. Original waveform series.

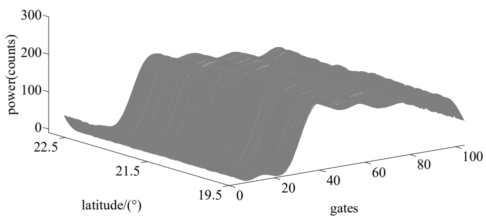

Figure 5. Reconstructed waveform series.

3.3Waveform retracking

Retracked the 20hz original waveforms and reconstructed waveforms by OCOG, threshold and 5-β algorithm respectively to get the midpoint of leading edge. The midpoints of leading edge obtained from original waveforms were recorded as Gr_1, and the reconstructed waveforms' midpoint of leading edge were recorded as Gr_2. Because the study area was dominated by ocean echoes, threshold factor took 50%[17]. The range correction obtained by waveform retracking was

$$dr = \Delta R \times \left(G_r - G_0 \right) \quad (14)$$

Where ΔR was the distance of one gate of the altimeter satellite, and the Jason-1 satellite's was 0.46875m. Gr was the actual midpoint of leading edge after waveform retracking. G_0 was the presupposed tracking gate, and the Jason-1 satellite's was 32.5. The slope of the leading edge of reconstructed waveform changed greatly compared with the original waveform, but the amplitude of the reconstructed waveform was more consistent with the original waveform. This paper performed cubic spline interpolation on the reconstructed waveform and the original waveform respectively, and found the power interpolation point corresponding to Gr_2 on reconstructed waveform, then found the point on original waveform that was the same or closest to this power interpolation point, and the gate interpolation point that corresponding to the power value on original waveform was used as a new leading edge midpoint, which was recorded as Gr_3. The range correction that corresponding to Gr_3 according to Equation 14 was calculated to investigate the effect of the slope change of the reconstructed waveform on the result. This method was referred to herein as "SSA retrack interpolation" algorithm. The technical flow chart corresponding to this study was shown in Figure 6.

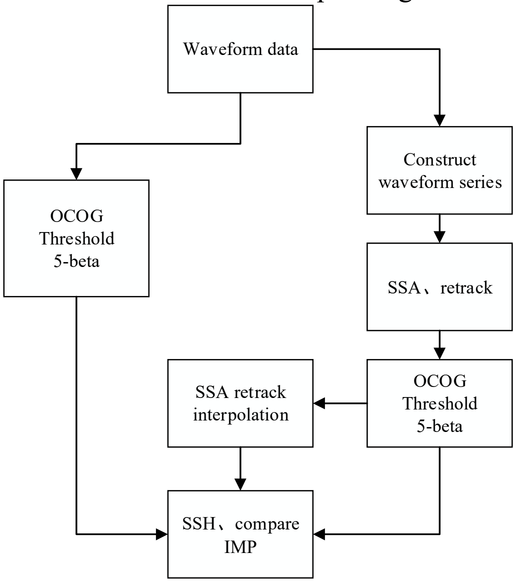

Figure 6. Technical flow chart.

3.4Waveform retracking result evaluation

SSH refers to the distance from sea surface to reference ellipsoid. It is affected by tides, gravity fields, ocean circulation, etc. The satellite altimeter didn't directly provide SSH data. SSH could be obtained by equation 15.

$$SSH = H_{alt} - H_{range} - \sum R_c \tag{15}$$

Where H_{alt} was the height of the Jason-1 satellite above the reference ellipsoid and H_{range} was the distance from satellite to sea surface in nadir point. $\sum R_c$ was the sum of the error corrections.

$$\sum R_c = R_{dry} + R_{wet} + R_{iono} + R_{ssb} + R_{inv} + R_{tid} + dr \tag{16}$$

Where R_{dry} was model dry tropospheric correction, R_{wet} was radiometer wet tropospheric correction, R_{iono} was ionospheric correction on Ku band, R_{ssb} was sea state bias correction in Ku band, R_{inv} was inverted barometer height correction, R_{tid} was tide correction, dr was correction of waveform retracking.

The IMP was used to judge the quality of SSH after waveform retracking[16], it was

$$IMP = \frac{\delta_{raw} - \delta_{retracked}}{\delta_{raw}} \times 100\% \tag{17}$$

Where δ_{raw} was the std(standard deviation) of the difference between the original SSH without waveform retracking and the Geoid that was calculated by EGM2008 model, $\delta_{retracked}$ was the std of the difference between SSH obtained by various waveform retracking methods and the Geoid. If the IMP was less than 0, it meant that the quality of SSH reduced, otherwise, the quality improved. Figure 7, Figure 8 and Figure 9 were the comparison of the original SSH and Geoid and the SSH calculated by 5-β parameter algorithm, OCOG, threshold and their improved methods. The Geoid was calculated by EGM2008 model. Table 1 showed the success rate of various waveform retracking methods and IMP.

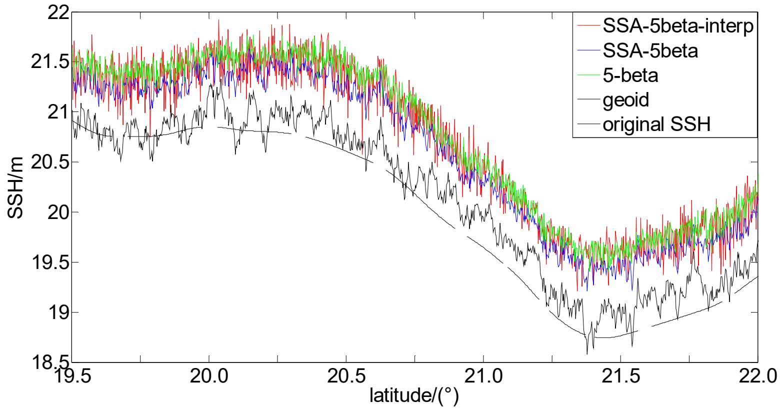

Figure 7. 5-β parameter algorithm and its improvements.

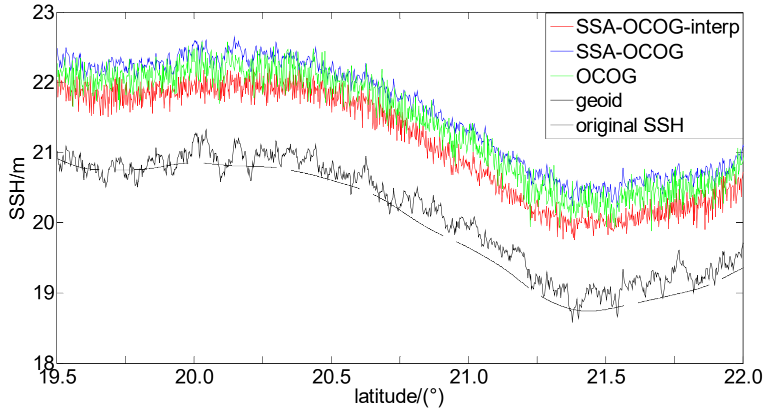

Figure 8. OCOG and its improvements.

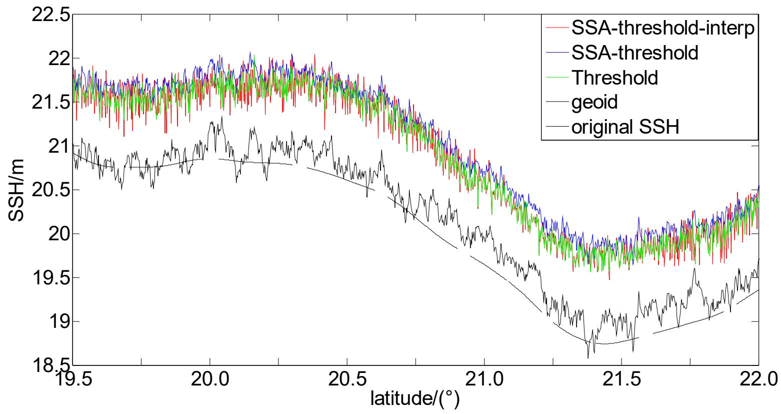

Figure 9. Threshold and its improvements.

Table 1. Comparison of waveform retracking results.

Waveform	Total number	Retracked	Retracked	δ_{raw}/m	$\delta_{retrack}$/m	IMP/

retracking methods	of wavefroms	waveform number	success rate (%)			(%)
5-β	1020	997	99.7	0.147	0.115	22.0
OCOG	1020	1020	100	0.147	0.176	-19.2
Threshold	1020	1020	100	0.147	0.122	17.5
SSA-$5-\beta$	1020	1020	100	0.147	0.113	23.1
SSA-OCOG	1020	1020	100	0.147	0.117	20.8
SSA-Threshold	1020	1020	100	0.147	0.107	27.3
SSA-$5-\beta$-intrep	1020	1020	100	0.147	0.189	-28.0
SSA-OCOG-interp	1020	1020	100	0.147	0.137	6.90
SSA-threshold-interp	1020	1020	100	0.147	0.163	-11.0

It could be seen from Table 1 that the success rate of the other retracking methods except 5-β algorithm was 100%. The experimental area selected in this paper was the deep sea area, and the success rate of 5-β algorithm was close to 100%. Among the three methods of 5-β, OCOG and threshold, the OCOG had the lowest IMP value that was less than 0, indicating that the retracking result of OCOG was the worst. This was because the OCOG algorithm used all waveform data to calculate the midpoint of leading edge, and the SSH obtained by OCOG was choppiest. 5-β algorithm and threshold had better results. The former had a larger IMP value than the latter, indicating that in the deep sea region, 5-β algorithm was better than threshold algorithm. The results showed that the IMP of SSH obtained by the combination of SSA and waveform retracking was larger than original one, and the OCOG had the largest improvement by SSA, mainly because the noise contained in the original waveforms was removed after SSA. Reconstructed waveforms became more regular, and OCOG was most sensitive to the signal-to-noise ratio, so it had the greatest improvement. Threshold method had the highest IMP value, because the leading edge of the reconstructed waveform was easier to identify, and the maximum amplitude was easier to determine. Among the combination of SSA and waveform retracking methods, 5-β and threshold algorithms were still the most accurate, and OCOG had the lowest accuracy. The IMP of the SSA retrack interpolation method was the lowest compared to other methods, indicating that this new method did not greatly improve the retracking result.

4. Conclusions

This paper proposed a new method that combining SSA and waveform retracking processed waveform data, and conducted an experimental study in the southwestern sea area of Taiwan island. The results showed that reconstructed waveform series obtained by SSA exhibited strong gradation, and the single waveform’s leading edge was easier to identify. Combine SSA and waveform retracking method to process waveform data could improve IMP value. Compared to SSA+OCOG, SSA+ 5-β and SSA+threshold had higher precision. It had been proved that the SSA retrack interpolation method had no better improvement on result.

This paper demonstrated the feasibility of processing waveform data by combining SSA and waveform retracking methods. At the same time, the method was to process the waveform series, which could fully consider the graduality of the waveforms, and had guiding significance for the subsequent research on the waveform retracking in the offshore area.

References

[1] Wang, G.Y., Wang, H.Y., Xu, G.C. (1995) The Theory of Satellite Altimetry. Science Press, Beijing.

[2] Fu, L.L., Cazenave, A. (2001) Satellite altimetry and earth sciences: a handbook of techniques and applications. Academic Press, San Diego.

[3] Wingham, D.J., Rapley, C.G., Griffiths, H. (1986) New techniques in satellite altimeter tracking systems. In: Pro IGARSS'86 Symp. Zurich. Pp. 1339-1344.
[4] Bamber, J.L. (1994) Ice sheet altimeter processing scheme. Int. J. Remote Sens., 15(4): 925-938.
[5] Laxon, S. (1994) Sea ice altimeter processing scheme at the EODC. Int. J. Remote Sens., 15(4): 915-924.
[6] Davis, C.H. (1997) A robust threshold retracking algorithm for measuring ice-sheet surface elevation change from satellite radar altimeter. IEEE Trans. Geosci. Remote. Sens.,35(4): 974-979.
[7] Hayne, G.S. (2003) Radar altimeter mean return waveforms from near- normal-incidence ocean surface scattering. IEEE Transactions on Antennas & Propagation., 28(5): 687-692.
[8] Martin, T.V., Brenner, A.C., Zwally, H.J., Bindschadler, R.A. (1983) Analysis and tracking of continental ice sheet radar altimeter waveforms. J. Geophys. Res., 88(C3): 1608-1616.
[9] Guo, J.Y., Gao, Y.G., Chang, X.T., Hwang, C.W. (2010) Optimal threshold algorithm of Envisat waveform retracking over coastal sea. Chinese J. Geophys., 53(4): 807-814.
[10] Yang, L., Lin, M.S., Zhuang, Y.G., et al. (2011) A retracking algorithm based on waveform classification and sub-waveform extraction for coastal altimetry. Sci. Sin. Terrae., 41: 1706-1713.
[11] Broomheada, D.S., King, G.P. (1986) Extracting qualitative dynamics from experimental data. Physica D., 20: 217-236.
[12] Wyatt, M.G., Kravtsov, S., Tsonis, A.A. (2012) Atlantic multi decadal oscillation and northern hemisphere's climate variability. Clim. Dynam., 38: 929-949.
[13] Chen, Q., Dam van, T., Sneeuw, N., et al. (2013) Singular spectrum analysis for modeling seasonal signals from GPS time series. J. Geodyn., 72: 25-35.
[14] Zabalza, J., Ren, J.C., Wang, Z., et al. (2014) Singular spectrum analysis for effective feature extraction in hyperspectral imaging., IEEE Geosci. Remote Sens., 11: 1886-1890.
[15] Kondrashov, D., Berloff, P. (2015) Stochastic modeling of decadal variability in ocean gyres. Geophys. Res. Lett., 42: 1543–1553.
[16] Hwang, C., Guo, J., Deng, X. (2006) Coastal gravity anomalies from retracked Geosat/GM altimetry: improvement, limitation and the role of airborne gravity data. J. Geod., 80: 204-216.
[17] Deng, X.L. (2004) Improvement of geodetic estimation in coastal regions from satellite radar altimetry. Curtin University of Technology, Perth.
[18] Hassani, H. (2007) Singular spectrum analysis: methodology and comparison. J. Data Science. 5: 239–257.